doi:10.1016/j.jmb.2004.12.020 J. Mol. Biol. (2005) 346, 745–759

JMB

Available online at www.sciencedirect.com

SCIENCE DIRECT®

ELSEVIER

Identification of Dynamical Correlations within the Myosin Motor Domain by the Normal Mode Analysis of an Elastic Network Model

Wenjun Zheng* and Bernard Brooks

Laboratory of Computational Biology, National Heart, Lung and Blood Institute, National Institutes of Health, Bethesda MD 20892, USA

**Corresponding author*

In order to systematically analyze functionally relevant dynamical correlations within macromolecular complexes, we have developed computational methods based on the normal mode analysis of an elastic network model. First, we define two types of dynamical correlations (fluctuation-based and density-based), which are computed by summing up contributions from all low-frequency normal modes up to a given cutoff. Then we use them to select dynamically important "hinge residues" whose elastic distortion affects the fluctuations of a large number of residues. Second, in order to clarify long-range dynamical correlations, we decompose the dynamical correlations to individual normal modes to identify the most relevant modes. We have applied these methods to the analysis of the motor domain of *Dictyostelium* myosin and have obtained the following three interesting results that shed light on its mechanism of force generation: first, we find the hinge residues are distributed over several key inter-subdomain joints (including the nucleotide-binding pocket, the relay helix, the SH1 helix, the strut between the upper 50 kDa and the lower 50 kDa subdomains), which is consistent with their hypothesized roles in modulating functionally relevant inter-subdomain conformational changes; second, a single mode 7 (for structure 1VOM) is found to dominate the fluctuation-based correlations between the converter/strut and the nucleotide-binding pocket, revealing a surprising simplicity for their intriguing roles in the force generation mechanism; finally, we find a negative density-based correlation between the strut and the nucleotide-binding pocket, which is consistent with the hypothesized signaling pathway that links the actin-binding site's opening/closing with the nucleotide-binding pocket's closing/opening.

Published by Elsevier Ltd.

Keywords: normal mode analysis; elastic network model; dynamical correlation; power-stroke; myosin

Introduction

New and existing crystal structures hint at working mechanism of myosin

All myosin motor domains with known structures consist of four subdomains (N terminal subdomain, upper 50 kDa subdomain or U50, lower 50 kDa subdomain or L50, and converter) connected by four flexible joints (relay helix, strut, SH1 helix, and switch II of the nucleotide-binding site).[1] These joints are believed to act together to control the overall organization of the motor domain and allow direct communication between distant regions such as nucleotide-binding site, the actin-binding interface and the converter/lever arm.

Analysis of existing crystal structures of myosins leads to their classification into the following states: the near-rigor state (PDB, 1MMA) is believed to be a weakly bound state that occurs shortly after detaching from actin;[2] the detached state (PDB, 1B7T) is argued to be a stable ATP state[1] with

Abbreviations used: PDB, Protein Data Bank; EM, electron microscopy; NMA, normal mode analysis; RMSF, root-mean-square fluctuation.

E-mail address of the corresponding author: zhengwj@helix.nih.gov

0022-2836/$ - see front matter Published by Elsevier Ltd.

unwound SH1 helix and unconstrained converter/lever arm; the transition state (PDB, 1VOM) is a pre-power-stroke, weakly bound state that occurs after hydrolysis.[3] Another way to classify those states is by using the open/closed states of switch I and II of the nucleotide-binding pocket:[4] the near-rigor state has switch I closed and switch II open and is therefore dubbed as state (C/O); similarly the transition state has both switch I and II closed so named as state (C/C). Two remaining states: (O/O) and (O/C) are hypothesized to exist as well.[4]

Recently, a new crystal structure[4] has been solved for the nucleotide-free motor domain of myosin II (PDB, 1Q5G) in which both switch I and II of the nucleotide-binding pocket have moved away from the nucleotide-binding positions, therefore it belongs to state (O/O). The above movement is linked with the rearrangement of the actin-binding region (the cleft between U50 and L50 subdomains). A communication pathway between the nucleotide-binding pocket and the actin-binding region is proposed: the binding with actin triggers the opening of the nucleotide-binding pocket and *vice versa*.

Another newly solved myosin V structure (PDB, 1OE9) reveals similar features as 1Q5G: the nucleotide-binding site has adopted new conformations that reduce the affinity for the nucleotide; the major cleft between U50 and L50 subdomains has closed after a significant rotation of the U50 subdomain by 25° relative to the N-terminal subdomain, and the lever arm has assumed a position consistent with that in an actomyosin rigor complex.[5]

The structures described above are believed to correspond to a strong actin-binding state without binding to MgADP, which may occur at the end of the power-stroke process after the release of phosphate and later MgADP.

Another clue to the above communication pathway was obtained by Himmel and co-workers:[6] they have analyzed the flexibility of switch I in the nucleotide-free near-rigor structure of scallop, and found that it was accompanied by a small rotation of the U50 subdomain that partly closed the U50–L50 cleft while opening the front door to the nucleotide-binding site; this rotation would not be possible if switch I were constrained by specific interactions with a nucleotide.

Meanwhile Volkmann and co-workers[7] have built two atomic models of myosin in acto-myosin complex using cryo-EM based quantitative fitting procedure: one in the presence and the other in the absence of MgADP. They have found the conformation of the MgADP state consists of a partially closed cleft and a downward position of the lever arm, while the MgADP-free rigor state shows a more tightly closed cleft with the lever arm moving even further down. A similar study[8] reported that the closing of the actin-binding cleft is structurally coupled to the opening of the nucleotide-binding pocket.

In addition to the pathway described above between the actin-binding site and the nucleotide-binding pocket, analysis of these myosin structures also suggests plausible linkage between the nucleotide pocket (closed/open) and the position of the force-generating lever arm being in the up or down position: in the near-rigor state, switch II is open, and the lever arm (or the converter if the lever arm is disordered, same below) is in down position; in the transition state both switches are closed and the lever arm (or the converter) is in the up position. In the new structures 1Q5G and 1OE9, the lever arm is also in the down position, preserving the correlation of an open switch II and the lever arm (or the converter) in the down position.

Motivated by the above observations for dynamical linkages among the nucleotide-binding site, the actin-binding site and the force-generating converter/lever arm, the following power stroke mechanism was proposed: right after the hydrolysis, actin binding triggers the opening of switch I which allows the release of phosphate (and ADP at a later time) and induces a power stroke, the swinging motion of the lever arm from the up to down orientation. During this transition, myosin goes from a weakly bound transition state to a strongly bound rigor state. A reverse stroke of the lever arm from the down to up orientation is expected to occur upon ATP binding. This power stroke picture is argued to hold for other motor proteins as well.[9]

However, controversies remain:

1. Kinetic study seems to suggest that strong binding with actin (a prerequisite for force generation) occurs after the swinging motion of the lever arm, consistent with a Brownian ratchet scenario instead of the power stroke picture.[10]
2. The power stroke scenario is essentially based on existing static crystal structures where several uncertainties remain: for example, actin binding is missing in those structures, and the lever arm orientation may be affected by passive bending at the pliant region due to crystal packing forces.[11]
3. Cryo-EM-based low-resolution models of acto-myosin complex only catch events at the end of the power stroke but not earlier in the stroke when myosin is not strongly bound to actin.

Finally, the hypothesized dynamical pathways linking different states remain to be further justified both experimentally and computationally.

Elastic network model applied to the study of motor proteins

Long-time simulation of myosin dynamics with atomic details is not feasible for modern computers. Normal mode analysis (NMA) based methods may avoid the need for very expensive computation by focusing on a small subset of low-frequency normal modes that are biologically relevant.[12–15] Recent work[16,17] has demonstrated that the observed conformational changes between different myosin

structures are well described by a limited number of low-frequency normal modes, in some cases even a single mode is good enough.[18] Despite these progresses, the mechanism of force generation in myosins remains to be clarified in details by NMA, partly for the lack of systematic computational methods that can analyze dynamical correlations based on NMA. Although some preliminary work[19] has been done to employ certain pair-wise correlation function such as $\langle \delta r_{ia} \delta r_{ja} \rangle$ to identify inter-domain and intra-domain correlations of collective motions, no systematic study has been performed. It is the purpose of this work to address this issue and develop computational tools based on NMA of an elastic network model that can analyze dynamical correlations systematically. First, we define and compute two types of dynamical correlations (density-based and fluctuation-based), then we apply them to the selection of dynamically important "hinge residues" and the description of their domains of correlation (see Materials and Methods). Second, we decompose the dynamical correlations to individual modes to identify the most relevant normal modes which facilitate the clarification of long-range allostery.

It has been widely conjectured that the motor proteins generate force *via* the transmission and amplification of the local changes in the nucleotide-binding pocket. In the context of the elastic network model, there are at least two possible ways by which the elastic network can propagate the local perturbation at the nucleotide-binding pocket to a remote site (for example, the actin-binding site and the converter/lever arm of myosin).

1. Density-based transmission: The local change takes the form of a distortional force between the ligand and the binding site, which is coupled to the local density of residues. It induces a number of normal modes that add up to a global conformational change of the motor domain that results in the transition of myosin from one equilibrium conformational state to another. This is reminiscent of the mechanical power-stroke scenario.[9]
2. Fluctuation-based transmission: The local change does not perturb the equilibrium state directly, instead it only affects the strength of fluctuation at the ligand-binding site, which is transmitted to remote sites by means of normal modes to induce changes in fluctuation there as well. This is reminiscent of a "modulated" Brownian search mechanism where the modulation from the ligand-binding site results in altered fluctuations instead of a change to the equilibrium state.

It is the purpose of this work to apply the NMA-based analysis of dynamical correlations to explore the two possibilities described above in the working mechanisms of myosin motors.

Results

To explore the dynamical correlations within the motor domain of myosins, we first employ the fluctuation-based correlation to identify critical hinge residues and their domains of correlation (see Materials and Methods); then we apply the mode-decomposition technique to several selected pair-wise correlations to identify the dominant normal modes; finally we will discuss the density-based correlation and its sign, which is of particular interest to the clarification of the hypothesized communication pathway between the actin-binding site and the nucleotide-binding site.

We will use the crystal structures of *Dictyostelium* myosin II (PDB, 1VOM, 1MMA, and 1Q5G) as test cases.

Multiple hinge motions of the myosin motor domain described by low-frequency normal modes

Before we go into the discussion of the dynamical correlations, we show in Table 1 the results of dynamical domain analysis for the ten lowest normal modes: for the conformational changes described by the eigenvector of each normal mode, the whole myosin motor is partitioned into several relatively rigid domains which undergo inter-domain hinge motions (see Materials and Methods). Indeed, multiple hinge motions involving the converter, the N-terminal subdomain, the U50 subdomain (especially the HCM loop) relative to the core domain are clearly revealed by analyzing those modes (for several examples, see Figure 1). The clarification of these highly complex collective motions demands the development of novel computational methods as we propose here.

Fluctuation-based correlation for *Dictyostelium* myosin

Finding hinge residues with high connectivity of dynamical correlation

By computing and sorting the connectivity of correlation for all residues of *Dictyostelium* myosin (see Materials and Methods) we find the hinge residues with high value of connectivity (top 10%, 74 in total) are mostly distributed over several key inter-subdomain joints (Figure 2): including the nucleotide-binding pocket (switch I and II, P loop), the relay helix, the SH1 helix, and the strut between the U50 and L50 subdomains. This is consistent with their hypothesized roles in modulating functionally relevant inter-subdomain conformational changes.[1] In order to validate those "hinge residues", we make cross-reference to the results of dynamical domains partition based on analyzing the conformational changes described by individual low-frequency normal modes (see Table 1).

We then analyze the domains of correlation (see Materials and Methods) for selected hinge residues

Table 1. Results of dynamical domain partition and hinge (bending) residues for the lowest ten normal modes obtained by DynDom[23]

Mode	Number of domains	Ranges of domains	Hinge residues
1	2	1:495–499,692–745	
		2:4–494,500–691	483–495,499–509,684–692
2	2	1:4–486,503–689	
		2:487–502,690–745	481–487,502–511,683–690
3	2	1:723–737	
		2:4–722,738–745	688–723,737–745
4	4	1:4–33,81–396,407–697,722–745	
		2:34–80	18–36,80–85
		3:397–406	395–397,406–408
		4:698–721	695–699,721–737
5	3	1:4–37,45–47,80–396,408–745	
		2:38–44,48–79	21–38,44–48,79–84
		3:397–407	395–397,407–416
6	2	1:4–695,722–741,745–745	
		2:696–721,742–744	689–696,720–742,744–745
7	4	1:4–18,33–218,230–262,435–588,619–695,734–741,743–745	
		2:19–32	16–19,32–34
		3:219–229,263–434,589–618	218–219,229–235,262–263,434–435,588–592,618–621
		4:696–721,742–742	695–696,720–745
8	3	1:4–18,34–699,723–745	
		2:19–33	17–19,33–36
		3:700–722	698–700,721–736
9	3	1:4–16,81–82,87–696,722–745	
		2:17–80,83–86	16–17,80–83,86–87
		3:697–721	693–698,721–745
10	3	1:4–16,31–396,407–745	
		2:17–30	16–19,30–33
		3:397–406	395–397,406–410

Column 1 gives the mode number; column 2 gives the number of dynamical domains obtained by analyzing the conformational change of the given mode; column 3 gives the residue range for each domain (domain 1 is the domain fixed for structural alignment); column 4 gives the residue ranges for the hinge residues.

(as representatives of all 74; see Figure 3): their importance is validated by their sequential conservation (see below for residues marked by an asterisk (*)). Intuitively, the domain of correlation includes residues whose fluctuation is effectively triggered by elastic distortions at the given hinge residue. They form an inter-weaving network *via* spatial contacts, where the hinge residue serves as the central hub.

We now go into a detailed discussion of some hinge residues and their domains of correlation.

The nucleotide-binding site. We examine three hinge residues (182, 233 and 463) which belong to three parts of the nucleotide-binding site: switch I (*233**, 231 and 232*), switch II (*463* and 461*) and P-loop (*182**) (see Figure 3).

1. Both 182 and 233 are mostly correlated with U50 and the N-terminal subdomain, while 463 is equally correlated with both U50 and L50 subdomains (and the strut between them). Therefore, perturbations due to nucleotide binding/releasing at switch I and P loop can affect the actin-binding U50–L50 cleft by changing the movement of the U50 subdomain, while perturbations at switch II do so by modulating the movements of both U50 and L50 subdomains. It was found that the actin-binding cleft is closed by a shift of mass from the U50 subdomain toward the cleft while the L50 subdomain remains anchored to actin.[7] Our result combined with the above finding seems to favor the hypothesized role of switch I instead of switch II in modulating the opening/closing of the U50–L50 cleft. Indeed a visual inspection of the crystal structure reveals that the above residues all sit at the hinge region near the bottom of the U50–L50 cleft; the residues of the switch I and P loop lie closer to the U50 subdomain than the L50 subdomain, which explains qualitatively its stronger influence to the U50's fluctuation than the L50's.
2. For all three residues the correlation with the converter is insignificant (below cutoff), suggesting no significant direct coupling between them; however, 182/233's correlation domains reach part of the SH1 helix and 463's correlation domain reaches the top of the relay helix, which facilitates an indirect coupling with the converter *via* these joints (see below). The presence of direct coupling between the nucleotide-binding pocket and the U50–L50 cleft and the absence of such coupling between the nucleotide-binding pocket and the converter may also be intuitively explained by the

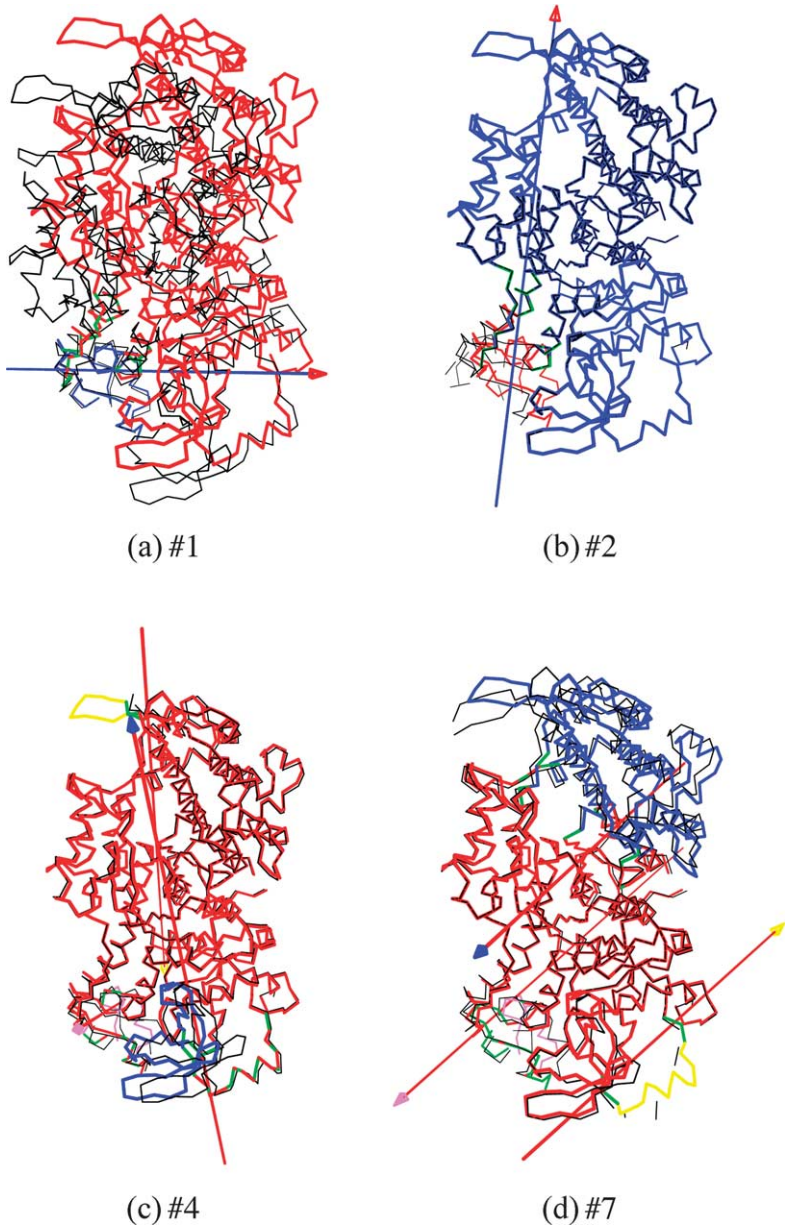

Figure 1. Conformational changes described by four low-frequency normal modes for *Dictyostelium* myosin (PDB code 1VOM). (a) Mode 1 describes a hinge motion between the converter and the core domain. (b) Mode 2 also describes a hinge motion between the converter and the core domain. (c) Mode 4 includes two hinge motions of the HCM loop (residues 397–406) and part of the N-terminal subdomain (residues 34–80) relative to the core domain. (d) Mode 7 includes three hinge motions that involve part of the N-terminal subdomain (residues 19–32), the U50 subdomain and the converter relative to the core domain. The crystal structure of 1VOM (colored) is superposed with the conformation obtained after a displacement given by the eigenvector of the given mode (black). The partition of dynamical domains (distinguished by different colors) was done by DynDom.[23] The hinge regions are colored green. The rotation axis for each pair-wise inter-domain motion is shown as an axis with an arrow head; the color of the axis stem is set to be the same as the domain fixed for the structural alignment, while the color of the arrow head is set to be the color of the moving domain.

following simple argument: the nucleotide-binding pocket sits exactly at the bottom joint/hinge between the U50 and L50 subdomains, which naturally controls the opening/closing of the U50–L50 cleft; however, it does not sit near any joint/hinge between the converter and any other subdomain, thus failing to effectively control the converter's hinge motion.

For validation, the analysis of mode 7 indeed reveals a hinge motion of the U50 subdomain, which is hinged at the nucleotide-binding site, in particular the switch I (see Figure 1(d) and Table 1).

The actin-binding site. We then examine the strut residues (*591*, 590*, 575*, 587*, 574*, 586*, 589, 573* and 629): 591 has strong correlation with switch I and II. This hints at the possibility of actin binding to modulate the opening/closing of the nucleotide-binding pocket, which is a reverse signaling pathway of the one discussed above. Therefore, our results support a bi-directional communication pathway between the U50–L50 strut and the nucleotide-binding site *via* two types of hinge motions: one is hinged at the bottom of the U50–L50 cleft near the nucleotide-binding site, and the other is at the top of the U50–L50 cleft near the strut.

For validation, the analysis of mode 7 reveals a shear motion of the U50 subdomain relative to the L50 subdomain, which significantly bends the strut (see Figure 1(d) and Table 1).

The converter. Then we examine 742*: surprisingly, its domain of correlation covers a wide range of residues including the P loop, switch II, relay helix, SH1 helix, and strut. This suggests the likelihood of force-generation to modulate the binding/releasing of nucleotide and even the opening/closing of the

Figure 2. Hinge residues identified in the structure of *Dictyostelium* myosin (PDB code 1VOM). Color blue/red corresponds to low/high value of connectivity of correlation. Labeled are the top 10% residues in order of descending connectivity: 693, 121, 689, 485, 505, 490, 508, 494, 692, 742, 231, 695, 591, 502, 739, 688, 506, 120, 691, 662, 503, 747, 660, 488, 272, 509, 234, 483, 683, 493, 420, 97, 487, 182, 486, 499, 500, 587, 484, 590, 489, 504, 629, 674, 266, 686, 233, 573, 432, 501, 651, 259, 122, 98, 687, 680, 574, 682, 158, 194, 262, 481, 491, 650, 675, 745, 586, 589, 216, 463, 510, 461 and 232.

U50–L50 cleft. This constitutes a reverse pathway of the widely hypothesized signaling pathway from the nucleotide-binding pocket down to the converter, although the latter is not supported by direct coupling of correlations as shown above. This is also consistent with the simple argument proposed above: namely, there is a hinge motion of the converter relative to the remaining subdomains, and 742 sits right at the hinge/joint between them.

For validation, we find several modes (3, 6, 7, and 9) involve a hinge motion of the converter subdomain hinged at 742 and neighboring residues (see Figure 1(d) and Table 1).

The relay helix. The relay helix contains a large number of hinge residues: 481, 483*, 484, *485*, 486, 487*, 488*, 489, 490*, 491, 493*, 494, 499, 500, 501, 502, 503, 504, *505*, 506*, 508, 509* and 510*, among which we examine 485 and 505. The 505's domain of correlation includes the nucleotide-binding pocket (P loop, switch II), the SH1 helix, and the converter. This hints at its plausible role of relaying dynamical correlation between the nucleotide-binding pocket and the converter. Similarly 485 is correlated with the P loop, switch II, SH1 helix and converter. This is not surprising, considering that the relay helix sits at the interface between the L50 subdomain and the converter. Therefore, it serves as a natural hinge/joint for the converter's hinge motion relative to the L50 subdomain.

For validation, we find that mode 1 and 2 support a hinge motion of the converter which is hinged at the relay helix (see Figure 1(a) and (b); Table 1).

The SH1 helix. The SH1 helix also contains a large number of hinge residues: *674*, 675*, 680*, 682*, 683*, 686, 687, 688, 689*, 691, 692, *693*, 695, among which we examine 674 (at the top of SH1 helix) and 693 (at the bottom of the SH1 helix and facing the converter). The 674's domain of correlation contains the nucleotide-binding pocket (switch I and switch II), the relay helix and the N-terminal subdomain; 693's domain of correlation includes the nucleotide-binding pocket (switch I and switch II), the relay helix and the converter. Similar to the case of the relay helix, this supports the possible role of SH1 helix in transmitting correlation between the nucleotide-binding pocket and the converter. This is again not surprising, considering that the SH1 helix sits at the interface between the U50 and N-terminal subdomains and the converter. Therefore it serves as a natural hinge/joint for the converter's hinge motion relative to the other two subdomains.

For validation, the analysis of several modes (1, 2, 3, 4, 6, 7, and 9) reveals a hinge motion of the converter which is hinged at the SH1 helix (see Figure 1 and Table 1).

Other hinge residues important to correlation transmission. There are other hinge residues besides the ones discussed above, for example some are at the interface between the N-terminal subdomain and the SH1 helix (including 97*, 98, 121, 120*, 122, 158), some are at the interface between the U50 and N-terminal subdomains which is hinge to the rotation of U50 relative to N-terminal subdomain (including 216, 272, 259, 262, 266, 420*, 432*, 660, 662*, 651*, 650*). Their functional roles are rarely discussed in the myosin literature, and they are worth further study.

To summarize, we have found significant fluctuation-based correlations within the motor domain of *Dictyostelium* myosin: the fluctuation at the actin-binding U50–L50 cleft (including the strut) is significantly correlated with the nucleotide-binding site; and the fluctuation of the converter is correlated with some important hinge residues at the

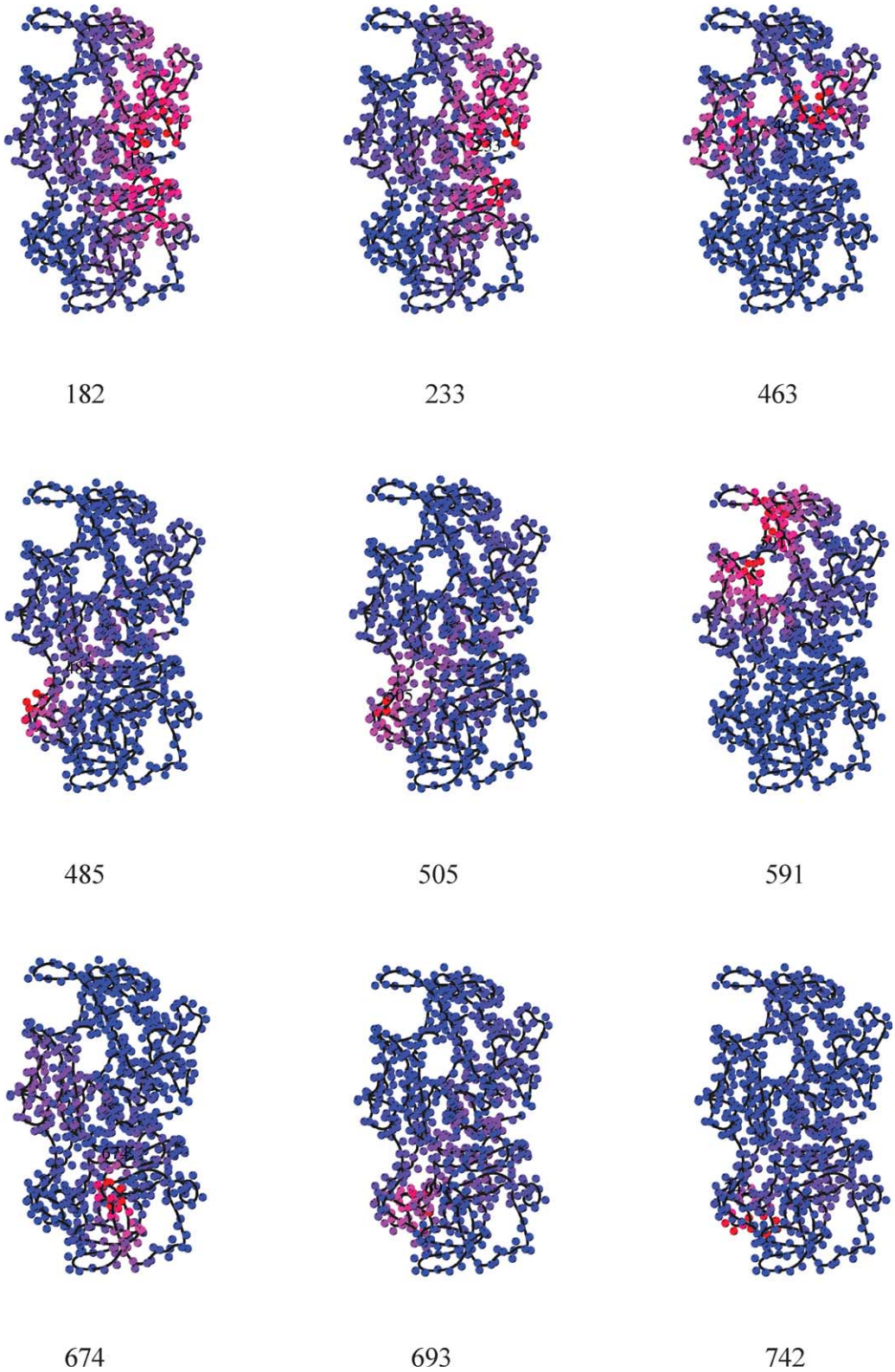

Figure 3. Domains of correlation for selected hinge residues of *Dictyostelium* myosin (PDB code 1VOM). Each panel shows the domain of correlation for one of the following hinge residues: 182, 233, 463, 485, 505, 591, 674, 693 and 742, respectively. Color blue/red corresponds to low/high value of C_{ij} (fluctuation-based correlation between residues i and j, where i is the residue being colored and j is the hinge residue).

Table 2. Results for the decomposition of the selected fluctuation-based correlations for *Dictyostelium* myosin between: 1, converter (740) and the nucleotide-binding pocket (182, 233, 463) and strut (591); 2, Strut (591) and the nucleotide-binding pocket (182, 233, 463)

PDB	Residue pair	Dominant mode (fractional contribution)
1VOM	740, 233	7(0.604)
	740, 182	7(0.752)
	740, 591	7(0.989)
	740, 463	7(1.308)
	591, 233	7(0.641)
	591, 182	7(0.499)
	591, 463	18(0.578)
1MMA	740, 233	3(0.515)
	740, 182	3(0.586)
	740, 591	3(1.232)
	740, 463	3(0.742)
	591, 233	14(0.515)
	591, 182	5(0.488)
	591, 463	15(0.417)
1Q5G	740, 233	1(0.869)
	740, 182	1(0.842)
	740, 591	1(0.496)
	740, 463	1(1.159)
	591, 233	8(1.261)
	591, 182	2(0.586)
	591, 463	14(0.387)

relay helix and the SH1 helix, and may be indirectly coupled to the remote nucleotide-binding pocket *via* these relays. The results are validated by comparing with the hinge residues identified by dynamical domains analysis based on analyzing the conformational changes described by each low-frequency normal mode. These results are also consistent with existing hypothesis[1] about the importance of these joint residues in modulating inter-subdomains conformational changes that are biologically important. This also supports the validity of the methods for identifying hinge residues that we introduced here. The hinge residues are promising targets for further study both experimentally and computationally.

Decomposition to individual modes

The fluctuation-based correlation as defined above is a summation of contributions from all modes below certain cutoff frequency. It decays rapidly as the pair-wise distance increases. Therefore, it can only capture direct short-range coupling between a hinge residue and those residues on the subdomain directly joining to the hinge residue; it, however, fails to identify more intricate long-range dynamical correlations through indirect couplings (for example the correlation from the nucleotide-binding site to the converter *via* the relay helix and SH1 helix). In order to analyze such long-range correlations, we introduce mode decomposition technique (see Materials and Methods) to analyze selected pair-wise correlations in order to find the dominant modes. The basic hypothesis is: there may only exist a handful of dominant low-frequency collective modes that may naturally account for long-range correlations.

We will focus on the following two classes of pair-wise correlations: the first is between the converter (site of fluctuation, represented by residue 740) and the nucleotide-binding pocket/strut (site of distortion, represented by residues 182, 233 and 463), and the second is between the strut (site of fluctuation, represented by residue 591) and the nucleotide-binding pocket (site of distortion). The results are summarized in Table 2 and Figure 4.

We find surprising simplicity underlying the mode-decomposition of the above fluctuation-based correlations as follows.

(a) Low-frequency modes (lower than mode 50) contribute most of the correlation for both classes (see Figure 4), strongly supporting the advantage of describing such long-range correlations with low-frequency normal modes computed from NMA: for *Dictyostelium* myosin with about 730 residues, only $50/(3\times730)\sim2\%$ of the whole normal mode space (with 3×730 modes in total) is relevant to the dynamical correlations we are interested in.
(b) Furthermore, in structure 1VOM a single normal mode (7) contributes most to both the above two classes of correlations, which unifies two separate pathways: one is between the converter and the nucleotide-binding pocket, and the other is between the strut and the nucleotide-binding pocket. Namely, this single mode 7 couples the nucleotide-binding pocket with both the strut at the actin-binding site and the force-generating converter, offering a simple picture for the complicated communication pathways among these three critical functional sites.

Similar results are found for the two other crystal structures 1MMA and 1Q5G: equivalent to mode 7 in 1VOM is mode 3 in 1MMA and mode 1 in 1Q5G (Table 2), which dominates the correlation between the converter and the nucleotide-binding pocket. We note, however, other modes contribute significantly to the correlation between the strut and the nucleotide-binding pocket, which hints at a decoupling between these two pathways. This may be caused by the structural difference between the two other structures and 1VOM: for example, in 1MMA and 1Q5G the converter is structurally less coupled with the relay helix than in 1VOM. This difference is also consistent with the uniqueness of the transition state as the pre-power-stroke state that is critical to the force generation mechanism.

A detailed analysis of the conformational change described by mode 7 (Figure 1(d)) confirms its critical role in sustaining the pathways among the actin-binding site, the nucleotide-binding site and the converter. Mode 7 simultaneously describes three hinge motions involving the U50 subdomain, the converter and part of the N-terminal subdomain relative to the core domain. Its bending/hinge

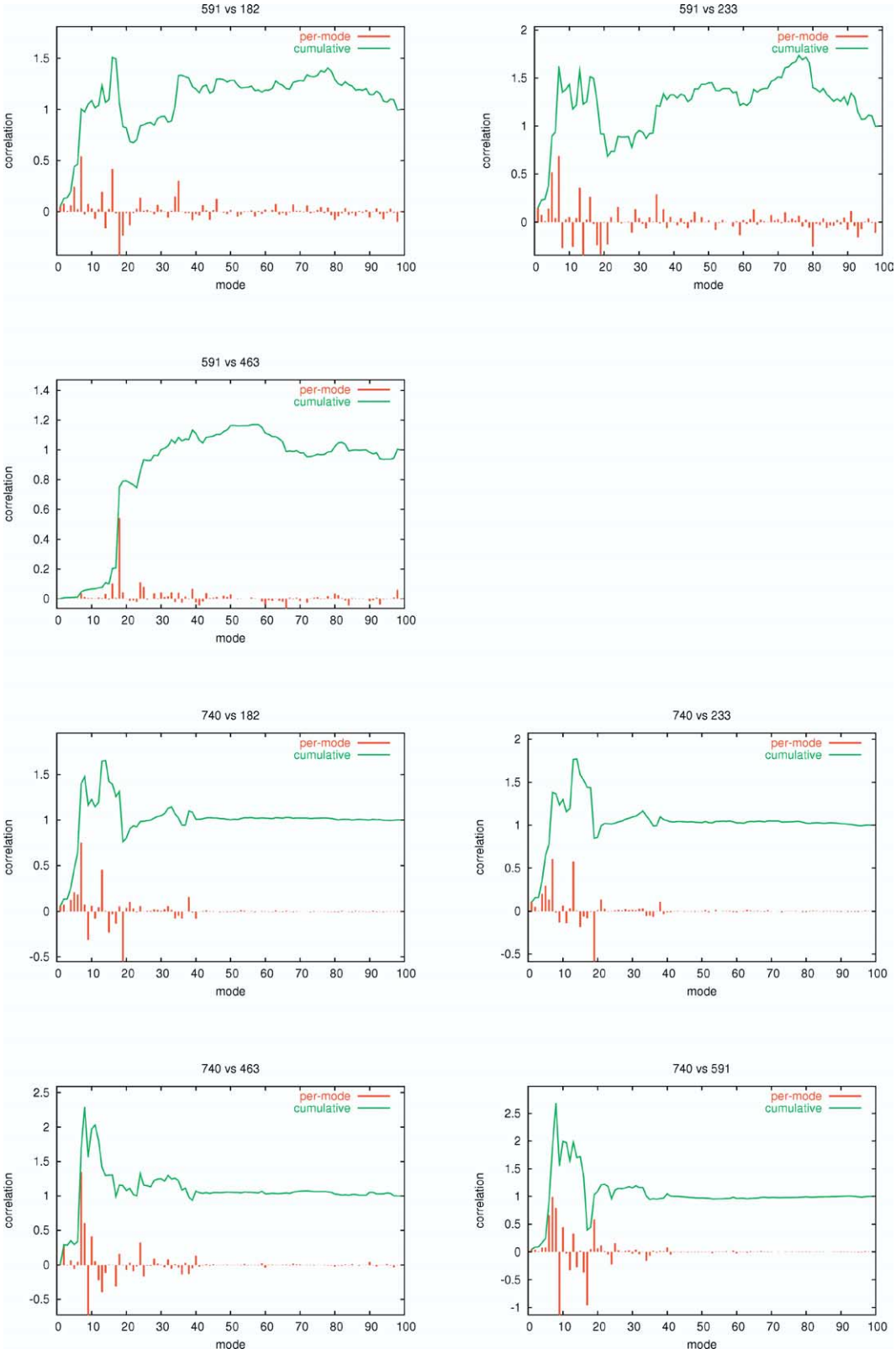

Figure 4. Results for the decomposition of the fluctuation-based correlations for *Dictyostelium* myosin (PDB code 1VOM). The correlation function is normalized by its value at the cutoff of mode 100. We show the correlations between the strut (591) and the nucleotide-binding pocket (182, 233, and 463), and the correlations between the converter (740) and the nucleotide-binding pocket (182, 233, and 463) plus strut (591). Green curves, cumulative contribution up to a given cutoff mode; red bars, fractional contribution from each given mode.

Table 3. Results for the decomposition of the density-based correlations for *Dictyostelium* myosin between the strut (591) and the nucleotide-binding pocket (182, 233, 463)

PDB	Pair	Sign	Dominant mode (fractional contribution)
1VOM	591, 233	−	7 (1.168)
	591, 182	−	7 (5.353)
	591, 463	+	17 (0.276)
1MMA	591, 233	−	5 (2.636)
	591, 182	−	5 (29.449)
	591, 463	+	5 (0.395)
1Q5G	591, 233	−	2 (0.598)
	591, 182	Mixed	2 (2.265)
	591, 463	−	13 (5.949)

residues are distributed over several key joints: including the U50–L50 strut, the switch I and II, P loop, the interface between the relay helix and the converter, etc. (Table 1). Although there exists lower modes (such as 1 and 2; see Figure 1(a) and (b)) that also describe hinge motions of the converter, they do not couple the converter to the other joints as mode 7 does and therefore contribute little to the above correlations. This remarkable result suggests that one single mode can indeed account for highly complicated motions of multiply coupled domains beyond single hinge motion; and the correlation-based decomposition technique is capable of identifying such important normal mode.

In summary, by applying the mode decomposition analysis to the above correlations, we obtain interesting results that are complimentary to those obtained from fluctuation-based correlation based on modes summation. Although we were unable to identify direct coupling between the converter and the nucleotide-binding pocket by using the latter method (see above), we are, however, able to reveal an interesting single mode dominance after the decomposition. This result supports the feasibility of analyzing certain selected normal modes to clarify a potentially complicated dynamical process involving coupled conformational changes of multiple domains.

Density-based correlation for *Dictyostelium* myosin

We now continue to study a new type of density-based correlation (see Materials and Methods) whose sign provides additional information about the nature of the correlation.

There has been an hypothesis on the following important pathways in myosin based on the available crystal structures.

1. The actin-binding U50–L50 cleft is hypothesized to be controlled by switch I opening/closing:[4] switch I opening induces the cleft closing and actin binding; inversely, actin binding triggers the opening of switch I to accelerate the release of phosphate.
2. The converter/lever arm are hypothesized to be controlled by the opening/closing of switch II, which initiates a series of conformational changes that induce their swinging motion.[4]

To test the above hypothesis, we analyze the density-based correlations for PDB structure 1VOM as follows. By perturbing the local density at the nucleotide-binding pocket, we simulate the effect of nucleotide binding or product release that induces closing/opening of the pocket. Then we study the response in density at a remote site (the U50–L50 strut or the converter–relay helix interface).

The results are summarized as follows (see Table 3 and Figure 5).

Actin-binding site versus *nucleotide-binding pocket*

The correlations between 591 of the strut and 233/182 of the nucleotide-binding pocket are both negative up to the cutoff at mode 100, and they are both dominated by mode 7. The latter (591 *versus* 182) is weaker quantitatively. The correlation between 591 and 463 is positive up to cutoff at mode 100, and it is contributed most by low-frequency modes below 40. The existence of a significant negative correlation between 591 and 233 is consistent with the hypothesized role of switch I's closing/opening in modulating the opening/closing of the actin-binding site. Furthermore the single-mode dominance by mode 7 is consistent with a similar observation in the fluctuation-based correlation discussed above.

Converter versus *nucleotide-binding pocket*

Contrary to the fluctuation-based correlation discussed above, here we find no simple pattern of correlation between 740 and 182/233/463: the correlation is strongly cutoff-dependent and has significant contribution from many modes up to cutoff at mode 100. This suggests that the density change at the converter–relay helix interface in response to the density change at the nucleotide-binding pocket is irregularly distributed among many normal modes, which is in contradiction with the predictable conformational change expected for a mechanic power-stroke.

We also analyze the two other structures (1MMA and 1Q5G) and find similar results. The correlation between 591 and 233 is negative, and there is no regular pattern of correlation between 740 and 182/233/463.

In summary, the hypothesized negative correlation between the nucleotide-binding pocket and the actin-binding site is supported by the above analysis of density-based correlation between the strut and switch I. However, we find no simple pattern of density-based correlation between the converter and nucleotide-binding pocket, in contrast to the simplicity revealed in the fluctuation-based correlations.

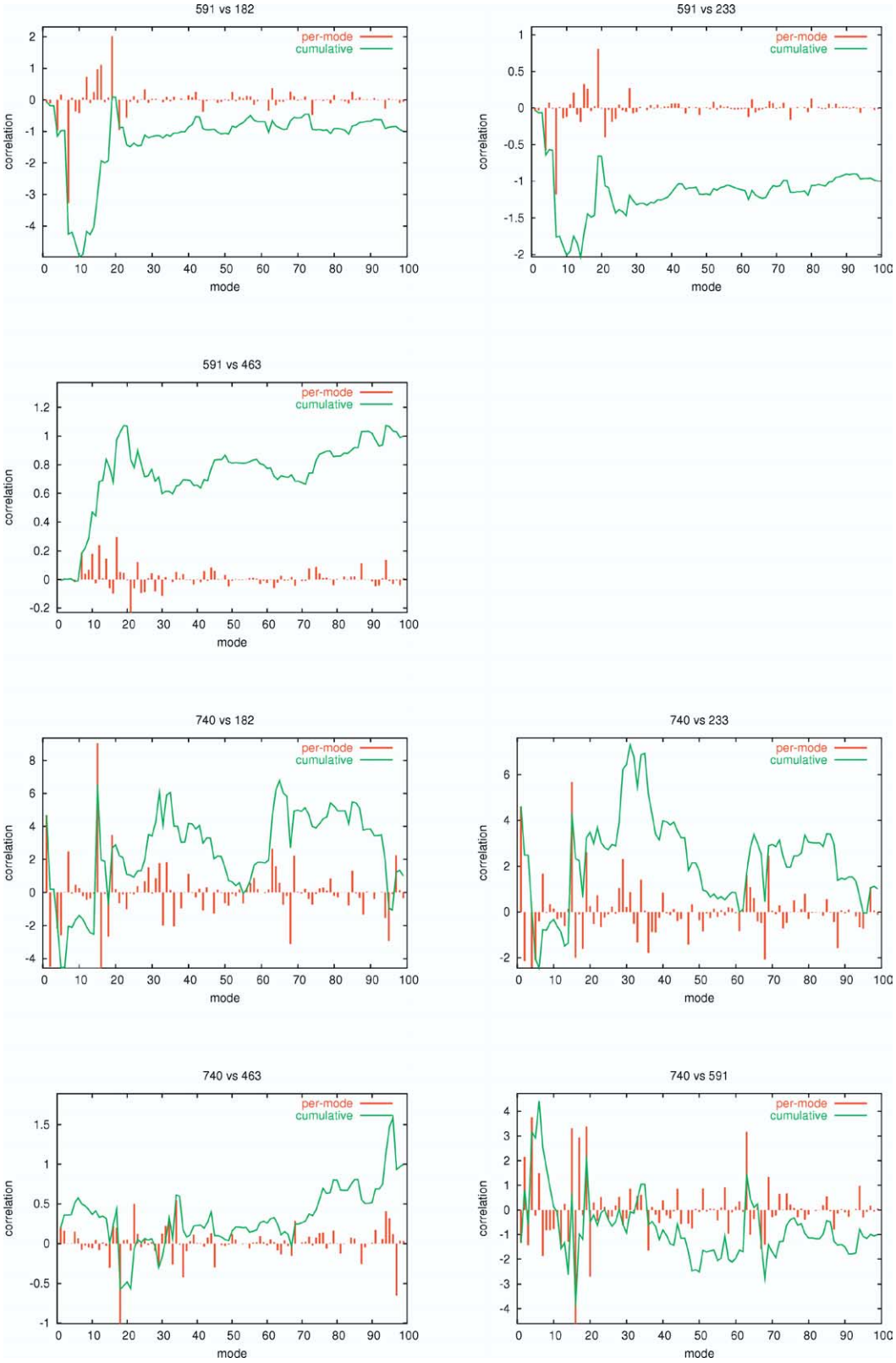

Figure 5. Results for the decomposition of density-based correlations for *Dictyostelium* myosin (PDB code 1VOM). The correlation function is normalized by its value at the cutoff of mode 100. We show the correlations between the strut (591) and the nucleotide-binding pocket (182, 233 and 463), and the correlations between the converter (740) and the nucleotide-binding pocket (182, 233 and 463) plus strut (591). Green curves, cumulative contribution up to a given cutoff mode; red bars, fractional contribution from each given mode.

Discussion

The study of both the fluctuation-based and the density-based correlations has yielded a comprehensive picture for the dynamical correlations within the myosin motor domain: the widely recognized negative correlation between the nucleotide-pocket's opening/closing and the actin-binding site's closing/opening is firmly supported by this analysis; meanwhile, the long-range fluctuation-based correlation between the nucleotide-binding site and the converter shows a surprising simplicity: it is dominated by a handful of low-frequency normal modes; in particular for 1VOM the dominant mode 7 also contributes most to the correlation between the nucleotide-binding pocket and the actin-binding site. Such simplicity does not exist for the density-based correlation.

The results described above shed some light on the controversy over the force-generation mechanism of myosins. First, the lack of simplicity in modes composition for the density-based correlation from the nucleotide-binding site to the converter casts doubt on the mechanical power-stroke scenario. Second, the simplicity in the channel of fluctuation-based correlation seems to suggest a simple mechanism of fluctuation-modulation from the ligand-binding site to the converter: the release of product enhances the flexibility of the nucleotide-binding pocket, which is transmitted as a perturbation to the converter to increase its fluctuation *via* a few low-frequency normal modes. This may partially contribute to the enhancement of a thermally driven Brownian search.

We acknowledge that the above observations are subject to the limits of our methodology. First, the effect of actin-binding is not modeled here and its relevance is not addressed. Second, the elastic network model only considers harmonic interactions, so the aharmonic effects (for example, multiple local minima, bias in directionality and irreversible conformational changes) are not properly accounted for, which may, however, be essential to substantiate the Brownian search scenario.

Recent studies by a number of researchers[12–19] have already demonstrated the feasibility of using just a couple of normal modes to capture the measured conformational changes of large protein complexes. Here on the same footing, we have found similar simplicity in using a handful of normal modes to capture biologically interesting dynamical correlations. There are additional advantages for this method. First, it does not require the prior knowledge of the relevant normal modes or the crystal structure of the end state, instead with a given crystal structure plus certain hypothesis about plausible sites involved in the correlation, we may be able to identify a few dominant modes which can be used to make new predictions that can be tested to further validate the hypothesis. Second, it is particularly useful when the measured conformational changes do not offer clear clues: for example, in case of myosin, a simple projection of the measured conformational changes (from 1VOM to 1MMA or 1Q5G) to individual modes points to the dominant mode 1 (with high overlap value), which, however, provides no clue about the coupling mechanism between the nucleotide-binding site, the actin-binding site and the converter because the former two are not coupled to the converter's motion by mode 1.

In conclusion, we have developed a novel computational method for calculating dynamical correlations, which can be used to analyze complicated dynamical processes involving coupled conformational changes of multiple domains. It is particularly helpful in analyzing a multi-subdomain complex such as the myosin motor domain, where multiple modes of hinge motions are possible.

After the completion of this work, we became aware of a recent work by Lavery and co-workers[22] that probed protein mechanics *via* local deformations, which is somehow related to the idea of computing dynamical correlation functions that are based on local deformations as well. Future exploration along this line, namely how proteins react structurally and dynamically to local deformations promises to reveal more and more insights for the dynamics and mechanics of macromolecular systems.

Materials and Methods

Elastic network model

Given the C^α atomic coordinates for a protein's native structure, we build an elastic network model by using a harmonic potential with a single force constant to account for pair-wise interactions between all C^α atoms that are within a cutoff distance ($R_C = 10$ Å). The energy in the elastic network representation of a protein is:

$$E_{\text{network}} = \frac{1}{2} \sum_{d_{ij}^0 < R_c} C(d_{ij} - d_{ij}^0)^2 \qquad (1)$$

where d_{ij} is the distance between the dynamical coordinates of the C^α atoms i and j, and d_{ij}^0 is the distance between C^α atoms i and j, as given in the crystal structure.

For the harmonic Hamiltonian in equation (1) we perform the standard normal mode analysis (NMA). The eigenvectors of the lowest frequency normal modes are used to interpret the protein conformational observed crystallographically.[12–18] The drastic simplification of representing the complex protein structure by an effective harmonic potential is justified by a study by Tirion[20] who showed that the use of a single spring constant reproduces the slow dynamics computed from the normal mode analysis of all-atom potentials. Hinsen[21] further simplified the elastic network model to the C^α only representation.

Dynamical correlation based on fluctuations in the C^α coordinates

Based on the NMA of the elastic network model[18] we can compute the root-mean-square fluctuation (RMSF) at

position i (the C^{α} position of residue i) as follows:

$$f_i = \langle \delta r_i^2 \rangle \propto \mathrm{Tr}(H^{-1})_{ii} = \sum_{a=x,y,z} H^{-1}_{ia,ia} = \sum_{1 \le m < M} \frac{v^m_{ia} \cdot v^m_{ia}}{\lambda_m} \quad (2)$$

where H^{-1} is the inverse of the Hessian matrix of the elastic network; λ_m and v^m_{ia} are the eigen-value and eigen-vector of mode m. A default cutoff at mode $M=100$ is used to compute H^{-1} (the results are robust to different selections of cutoff); and the six zero modes corresponding to rotations and translations are excluded (the non-zero modes start from 1). We note that equation (2) is only approximate given the system energy as in equation (1) where a-harmonic contributions are ignored. For simplification in notation, a factor of T/C is omitted in equation (2) (T is the temperature, C is the spring constant).

The RMSF is related to the B factor as follows:

$$B_i = \frac{8\pi^2}{3} f_i \quad (3)$$

We now introduce a perturbation at position j and study the change of f_i as response.

The simplest quadratic perturbation at position j to the total interaction energy is $\delta E^j = \delta r_j^2/2$, which effectively reduces the coordinate fluctuation at position j. The corresponding Hessian matrix elements read:

$$\delta H^j_{ka,lb} = \frac{\partial^2 \delta E^j}{\partial x_{ka}\, \partial x_{lb}} \quad (4)$$

which is 1 only if $k=l=j$ and $a=b$, and zero otherwise.

Then the change of f_i in response to this perturbation is:

$$\delta f_{i|j} \propto -\mathrm{Tr}(H^{-1} \delta H^j \cdot H^{-1})_{ii} = -\sum_{a,b=x,y,z} (H^{-1}_{ia,jb} \cdot H^{-1}_{jb,ia}) \propto -\sum_{a,b} \langle \delta r_{ia} \delta r_{jb} \rangle^2 \quad (5)$$

After normalization we can define the following pair-wise dynamical correlation between i and j:

$$C_{ij} = \frac{-\delta f_{i|j}}{f_i f_j} \quad (6)$$

Despite its simplicity, this result has one serious problem: δH^j as defined above does not preserve the translational and rotational symmetry, and there is non-zero coupling between the six trivial modes and the rest of the spectrum by δH^j; therefore, by simply excluding six zero modes from the calculation of H^{-1}, we effectively project δH^j to the subspace spanned by $3N-6$ normal modes as follows:

$$\delta H^j_{\mathrm{P}} = \delta H^j - \sum_{m=6 \text{ zero modes}} ((v^m)^{\mathrm{T}} \cdot \delta H^j \cdot v^m) \cdot v^m \cdot (v^m)^{\mathrm{T}} \quad (7)$$

The additional term introduces artificial off-diagonal matrix elements which lead to artificial long-range coupling in δH^j.

To avoid the above problem we introduce the following translationally and rotationally invariant perturbation at position j (it perturbs the spring constant of the springs connecting $C_{\alpha j}$ to its neighbors within 10 Å):

$$\delta E^j = \sum_{k:d_{\mathrm{kj}}<10} \frac{\delta r^2_{\mathrm{kj}}}{2} \quad (8)$$

and the corresponding Hessian matrix elements can be calculated as follows:

$$\delta H^j_{\mathrm{ka,lb}} = \frac{\partial^2 \delta E^j}{\partial x_{\mathrm{ka}} \partial x_{\mathrm{lb}}} \quad (9)$$

Then the change of f_i in response to δH^j is:

$$\delta f_{i|j} \propto -Tr(H^{-1} \delta H \cdot H^{-1})_{ii} = -\sum_{l,k;a,b,c=x,y,z} (H^{-1}_{\mathrm{ia,lb}} \cdot \delta H^j_{\mathrm{lb,kc}}\, H^{-1}_{\mathrm{kc,ia}}) \propto -\sum_{m,n} \frac{v^m_{\mathrm{ia}} \cdot \delta H^j_{\mathrm{mn}} \cdot v^n_{\mathrm{ia}}}{\lambda_m \lambda_n} \quad (10)$$

Then we can define the following pair-wise dynamical correlation between i (site of fluctuation) and j (site of distortion/perturbation):

$$C_{ij} = \frac{\delta f_{i|j}}{f_i} \quad (11)$$

There are the following sum rules:

$$\sum_j \delta f_{i|j} = f_i, \quad \sum_i \delta f_{i|j} = \sum_m \frac{\delta H^j_{mm}}{\lambda_m^2} \quad (12)$$

Physically, C_{ij} measures the fractional contribution by residue j to the RMSF at position i.

Now we use the fluctuation-based dynamical correlation to identify hinge residues as described by the following procedure.

First, we define and compute the connectivity of correlation for residue i (N_i): it is the number of residue j with C_{ji} higher than the cutoff value C_{cutoff}. C_{cutoff} is set to be the averaged value of C_{ij} for pairs of residues i and j separated by 10 Å ($C_{\mathrm{cutoff}} = \langle C_{ij} \rangle_{d_{ij}=10}$). N_i counts the number of residues whose fluctuation is significantly affected by a perturbation to residue i. These residues constitute the domain of correlation for residue i. Finally, we rank all residues by their connectivity of correlation N_i and select the top 10% of these as the set of hinge residue.

In order to validate the hinge residues identified as described above, we make comparison with the results of dynamical domains analysis based on analyzing the inter-domain conformational changes described by each low-frequency normal mode where hinge residues associated with specific hinge motions can be identified. This analysis is done by a computational tool called DynDom developed by Hayward†.[23]

Intuitively, the hinge residues with high connectivity of correlation serve as important hubs for signal transmission. These hinge residues are critically involved in the distortions required for triggering global conformational changes. The domain of correlation contains residues whose fluctuation is effectively triggered by distortions at the given hinge residue. This protocol provides a way of identifying hinge residues and their domains of correlation without specifying any particular normal mode. This is suitable for analyzing multi-domain structures where multiple hinge-motions are plausible. We note that the domain of correlation of residue i is very different from the set of residues physically connected by springs to residue i: the former usually encloses the latter and can cover a much larger region beyond 10 Å cutoff.

Dynamical correlation based on density of C^{α} atoms

The fluctuation-based correlation as defined above only concerns the amplitude of correlation but not its sign, because the perturbation introduced above does not

† This is downloadable from: http://www.sys.uea.ac.uk/~sjh/DynDom/dyndom.home.html

Table 4. Ranges of residue numbers for several important sites of *Dictyostelium* myosin

Strut	P loop	Switch I	Switch II	Relay helix	SH1 helix	Converter
590–593	179–186	233–238	454–459	466–518	669–690	710–747

perturb the equilibrium state and it always reduces the RMSF. There exist other correlation functions whose sign is as important as its amplitude. We now introduce one of them, the density-based correlation.

We define the local density function at position i:

$$\rho_i = \sum_j \exp\left(-\frac{r_{ij}^2}{2R_c^2}\right) \tag{13}$$

where R_c is the "radius" of residue j (R_c=5 Å). Here we assume each residue is represented as a 3D Gaussian distribution of density centered at the C^α atom.

At first order perturbation, the density change $\delta\rho_i$ is linearly related to the changes of the pair-wise distances δr_{ij} as follows:

$$\delta\rho_i = -\sum_j \frac{r_{ij}}{R_c^2}\exp\left(-\frac{r_{ij}^2}{2R_c^2}\right)\delta r_{ij} \tag{14}$$

Physically, a positive/negative change in the local density at position i signals the closing/opening of the pocket centered at position i.

The change of ρ_i due to a perturbation of density at position j (ρ_j) is given by the following density–density correlation function:

$$\langle \delta\rho_i\ \delta\rho_j\rangle = \sum_{1\le m<M} \frac{\delta\rho_i^m\ \delta\rho_j^m}{\lambda_m} \tag{15}$$

where the summation is over all low-frequency normal modes up to mode M (we use M=100 as default). Unlike the perturbation introduced in the definition of the fluctuation-based correlation, the perturbation to local density is coupled to a local distortional force that perturbs the equilibrium state of the system; and additional information is carried by the sign of correlation: for example, a negative density-based correlation between two sites dictates that when one of them opens the other would close; and a positive correlation means that both sites open/close together. This provides critical test on hypothesized pathways that correlate structural changes at one site with another: the correct pathway should be consistent with the sign of the computed correlation.

Decomposition of dynamical correlation to individual modes

Given the definitions of the above two dynamical correlations, it is straightforward to calculate the fractional contribution from each individual normal mode m ($m\le$100) as follows:

$$\delta f_{i|j,m} = \frac{\delta f_{i|j,\text{cutoff}=m} - \delta f_{i|j,\text{cutoff}=m-1}}{\delta f_{i|j,\text{cutoff}=100}} \tag{16}$$

$$\langle \delta\rho_i\ \delta\rho_j\rangle_m = \frac{\delta\rho_i^m\ \delta\rho_j^m/\lambda_m}{\langle \delta\rho_i\ \delta\rho_j\rangle|_{\text{cutoff}=100}} \tag{17}$$

Therefore, we can analyze which modes contribute most significantly to a given pair-wise correlation.

The analysis of dynamical correlation decomposed in the normal mode space carries significant value in the study of long-range correlations. In the coordinate space, the spatial correlation between position i and j as defined above contains the summation of all modes up to a cutoff frequency. Therefore, in order to yield significant value of correlation, "inter-modes cooperation" is required instead of "single-mode dominance". Namely, there needs to be a significant fraction of all modes up to the cutoff with significant positive contribution to the total correlation; otherwise, if only a small number of modes dominate, the summation in the numerator of $\delta f_{i|j}/f_i$ will be outweighted by the summation in its denominator as the cutoff becomes large. Meanwhile, the extent of inter-modes cooperation decays rapidly as d_{ij} increases. Therefore, the goal of identifying long-range correlations is at odds with the procedure of summation over all modes below a cutoff. Here the decomposition technique avoids the above problem, and it is able to select a few dominant modes for a chosen pair-wise correlation, which could provide a simplified picture for a seemingly intricate long-range correlation.

The selection criteria for interesting pair-wise correlations is as follows: for a pair of residues to be selected, one of them (site of distortion/perturbation) is one of those hinge residues as selected above, and the other (site of fluctuation) is from a subdomain or structural element which is hypothesized to be relevant to the force-generation function of myosins (for example, the converter, and the key inter-subdomains joints).

Definition of important sites of myosin

The ranges of residue numbers for several important sites in the myosin II motor domain are listed in Table 4; among them, the P loop, switch I and switch II constitute the nucleotide-binding site; the strut is a connector between the U50 and L50 subdomains, and its change allows a large number of direct interactions between them. There are two other critical joints: the relay helix connects the L50 subdomain with the force-generating converter, and the SH1 helix sits between the N-terminal subdomain and the converter.

Acknowledgements

This work is supported by the National Institutes of Health. We thank Dr Thirumalai from University of Maryland for discussions.

References

1. Houdusse, A., Szent-Gyorgyi, A. G. & Cohen, C. (2000). Three conformational states of scallop myosin S1. *Proc. Natl Acad. Sci. USA*, **97**, 11238–11243.
2. Gulick, A. M., Bauer, C. B., Thoden, J. B. & Rayment, I. (1997). X-ray structures of the MgADP,

MgATPgammaS, and MgAMPPNP complexes of the *Dictyostelium discoideum* myosin motor domain. *Biochemistry*, **36**, 11619.
3. Smith, C. A. & Rayment, I. (1996). X-ray structure of the magnesium (II)·ADP·vanadate complex of the *Dictyostelium discoideum* myosin motor domain to 1.9 Å resolution. *Biochemistry*, **35**, 5404.
4. Reubold, T. F., Eschenburg, S., Becker, A., Kull, F. J. & Manstein, D. J. (2003). A structural model for actin-induced nucleotide release in myosin. *Nature Struct. Biol.* **10**, 826–830.
5. Coureux, P. D., Wells, A. L., Menetrey, J., Yengo, C. M., Morris, C. A., Sweeney, H. L. & Houdusse, A. (2003). A structural state of the myosin V motor without bound nucleotide. *Nature*, **425**, 419–423.
6. Himmel, D. M., Gourinath, S., Reshetnikova, L., Shen, Y., Szent-Gyorgyi, A. G. & Cohen, C. (2002). Crystallographic findings on the internally uncoupled and near-rigor states of myosin: further insights into the mechanics of the motor. *Proc. Natl Acad. Sci. USA*, **99**, 12645–12650.
7. Volkmann, N., Hanein, D., Ouyang, G., Trybus, K. M., DeRosier, D. J. & Lowey, S. (2000). Evidence for cleft closure in actomyosin upon ADP release. *Nature Struct. Biol.* **7**, 1147–1155.
8. Holmes, K. C., Angert, I., Kull, F. J., Jahn, W. & Schroder, R. R. (2003). Electron cryo-microscopy shows how strong binding of myosin to actin releases nucleotide. *Nature*, **425**, 423–427.
9. Vale, R. D. & Milligan, R. A. (2000). The way things move: looking under the hood of molecular motor proteins. *Science*, **288**, 88–95.
10. Houdusse, A. & Sweeney, H. (2001). Myosin motors: missing structures and hidden springs. *Curr. Opin. Struct. Biol.* **11**, 182–194.
11. Gourinath, S., Himmel, D. M., Brown, J. H., Reshetnikova, L., Szent-Gyorgyi, A. G. & Cohen, C. (2003). Crystal structure of scallop Myosin s1 in the pre-power stroke state to 2.6 Å resolution: flexibility and function in the head. *Structure (Camb.)*, **11**, 1621–1627.
12. Delarue, M. & Sanejouand, Y. H. (2002). Simplified normal mode analysis of conformational transitions in DNA-dependent polymerases: the elastic network model. *J. Mol. Biol.* **320**, 1011–1024.
13. Tama, F. & Sanejouand, Y. H. (2001). Conformational change of proteins arising from normal mode calculations. *Protein Eng.* **14**, 1–6.
14. Xu, C., Tobi, D. & Bahar, I. (2003). Allosteric changes in protein structure computed by a simple mechanical model: hemoglobin T↔R2 transition. *J. Mol. Biol.* **333**, 153–168.
15. Krebs, W. G., Alexandrov, V., Wilson, C. A., Echols, N., Yu, H. & Gerstein, M. (2002). Normal mode analysis of macromolecular motions in a database framework: developing mode concentration as a useful classifying statistic. *Proteins: Struct. Funct. Genet.* **48**, 682–695.
16. Navizet, I., Lavery, R. & Jernigan, R. L. (2004). Myosin flexibility: structural domains and collective vibrations. *Proteins: Struct. Funct. Genet.* **54**, 384–393.
17. Li, G. & Cui, Q. (2004). Analysis of functional motions in Brownian molecular machines with an efficient block normal mode approach: myosin-II and Ca^{2+}-ATPase. *Biophys. J.* **86**, 743–763.
18. Zheng, W. & Doniach, S. (2003). A comparative study of motor-protein motions by using a simple elastic-network model. *Proc. Natl Acad. Sci. USA*, **100**, 13253–13258.
19. Bahar, I., Erman, B., Jernigan, R. L., Atilgan, A. R. & Covell, D. G. (1999). Collective motions in HIV-1 reverse transcriptase: examination of flexibility and enzyme function. *J. Mol. Biol.* **285**, 1023–1037.
20. Tirion, M. M. (1996). Large amplitude elastic motions in proteins from a single-parameter, atomic analysis. *Phys. Rev. Letters*, **77**, 1905–1908.
21. Hinsen, K. (1998). Analysis of domain motions in large proteins. *Proteins: Struct. Funct. Genet.* **33**, 417–429.
22. Navizet, I., Cailliez, F. & Lavery, R. (2004). Probing protein mechanics: residue-level properties and their use in defining domains. *Biophys. J.* **87**, 1426–1435.
23. Hayward, S. & Berendsen, H. J. (1998). Systematic analysis of domain motions in proteins from conformational change: new results on citrate synthase and T4 lysozyme. *Proteins: Struct. Funct. Genet.* **30**, 144–154.

Edited by M. Levitt

(Received 19 October 2004; received in revised form 6 December 2004; accepted 9 December 2004)